J Neurooncol (2012) 109:521–527
DOI 10.1007/s11060-012-0918-0

CLINICAL STUDY

Molecular imaging of pediatric brain tumors: comparison of tumor metabolism using ^{18}F-FDG-PET and MRSI

Sean J. Hipp · Emilie A. Steffen-Smith · Nicholas Patronas · Peter Herscovitch · Jeffrey M. Solomon · Robyn S. Bent · Seth M. Steinberg · Katherine E. Warren

Received: 2 March 2012 / Accepted: 19 June 2012 / Published online: 4 July 2012

Abstract Magnetic resonance spectroscopic imaging (MRSI) and ^{18}F-fluorodeoxyglucose positron emission tomography (FDG-PET) are non-invasive imaging techniques routinely used to evaluate tumor malignancy in adults with brain tumors. We compared the metabolic activity of pediatric brain tumors using FDG-PET and MRSI. Children ($n = 37$) diagnosed with a primary brain tumor underwent FDG-PET and MRSI within two weeks of each other. Tumor metabolism was classified as inactive, active or highly active using the maximum choline:*N*-acetyl-asparate (Cho:NAA) on MRSI and the highest tumor uptake on FDG-PET. A voxel-wise comparison was used to evaluate the area with the greatest abnormal metabolism. Agreement between methods was assessed using the percent agreement and the kappa statistic (κ). Pediatric brain tumors were metabolically heterogeneous on FDG-PET and MRSI studies. Active tumor metabolism was observed more frequently using MRSI compared to FDG-PET, and agreement in tumor classification was weak ($\kappa = 0.16$, $p = 0.12$), with 42 % agreement (95 % CI = 25–61 %). Voxel-wise comparison for identifying the area of greatest metabolic activity showed overlap in the majority (62 %) of studies, though exact agreement between techniques was low (29.4 %, 95 % CI = 15.1–47.5 %). These results indicate that FDG-PET and MRSI detect similar but not always identical regions of tumor activity, and there is little agreement in the degree of tumor metabolic activity between the two techniques.

Sean J. Hipp and Emilie A. Steffen-Smith contributed equally to this study.

S. J. Hipp · E. A. Steffen-Smith · R. S. Bent
Pediatric Oncology Branch, Center for Cancer Research, National Cancer Institute, National Institutes of Health, 9000 Rockville Pike, Bethesda, MD 20892, USA

S. J. Hipp
Department of Pediatrics, San Antonio Military Medical Center, 3551 Roger Brooke Dr., Ft. Sam Houston, TX 78234, USA

S. J. Hipp
Department of Pediatrics, Walter Reed National Military Medical Center, 8901 Rockville Pike, Bethesda, MD 20889, USA

S. J. Hipp
Department of Pediatrics, Uniformed Services University of the Health Sciences, 4301 Jones Bridge Road, Bethesda, MD 20814, USA

N. Patronas · J. M. Solomon
Department of Radiology & Imaging Sciences, Clinical Center, National Institutes of Health, 9000 Rockville Pike, Bethesda, MD 20892, USA

P. Herscovitch
PET Department, Clinical Center, National Institutes of Health, 9000 Rockville Pike, Bethesda, MD 20892, USA

J. M. Solomon
Expert Image Analysis, LLC, 12609 Orchard Brook Terrace, Potomac, MD 20854, USA

S. M. Steinberg
Biostatistics and Data Management Section, Center for Cancer Research, National Cancer Institute, National Institutes of Health, 9000 Rockville Pike, Bethesda, MD 20892, USA

K. E. Warren (✉)
Pediatric Oncology Branch, Center for Cancer Research, National Cancer Institute, National Institutes of Health, Building 10/Room 1-5750, 9000 Rockville Pike, Bethesda, MD 20892, USA
e-mail: warrenk@mail.nih.gov

Keywords Pediatric · Brain tumor · ^{18}F-FDG-PET · MR spectroscopy · Metabolism

Introduction

Primary central nervous system (CNS) tumors are the most common solid tumors in children. Management of these patients can be challenging, as treatment is highly dependent on tumor histology, location, and patient age [1]. The location and pathology of these tumors are heterogeneous [2], and in many cases, proximity to critical brain structures precludes resection or diagnostic biopsy. MRI cannot always distinguish treatment effects such as radiation necrosis from recurrent disease [3, 4]. Application of functional and molecular imaging techniques, including magnetic resonance spectroscopic imaging (MRSI) and ^{18}F-fluorodeoxyglucose positron emission tomography (FDG-PET) may improve management in this population by providing noninvasive assessment of tumor biology. MRSI provides biochemical information on tissue metabolism. In pediatric CNS tumors, changes in MRSI metabolites have been predictive of tumor grade, tumor progression and overall patient survival [5–10]. FDG-PET imaging reflects tissue metabolism through the uptake of ^{18}F-fluorodeoxyglucose (FDG). In adult brain tumors, FDG-PET is used in combination with MRI to predict tumor grade and assess response to therapy [11–16]. The clinical value of FDG-PET in pediatric brain tumor patients is less firmly established. However, several studies indicate that FDG-uptake in pediatric brain tumors is prognostic and may assist in selection of biopsy targets and identification of margins for tumor resection [17–20].

While MRSI and FDG-PET provide insight to the metabolic behavior of brain tumors, the association between the information obtained from each is unclear. The objective of this study was to compare MRSI and FDG-PET in the determination of tumor metabolism in children with primary brain tumors.

Materials and methods

Patients

Pediatric patients (ages $\geq$1 to $\leq$21 years) referred to our institution for evaluation of a brain tumor were eligible for NCI study NCT00067821 (www.clinicaltrials.gov). Information regarding tumor diagnosis was provided by the referring institution. Patients with any type of brain tumor or residual lesion after treatment for a brain tumor were eligible. Prior and concurrent treatment was permitted, provided measurable or evaluable residual signal abnormality was confirmed on the patient's most recent radiographic evaluation. Exclusion criteria included history of diabetes or steroid-induced hyperglycemia (fasting glucose >150 mg/dL), history of severe reaction to imaging contrast agents and inability to complete FDG-PET or MRI study due to physical restriction. Patients <18 years had a weight requirement of <70 kg to receive standard FDG dosimetry allowed for research; patients whose weight exceeded the PET scanner's maximum limit (>136 kg) were excluded. The institutional review board and radiation safety committee approved the study. All patients or their legal guardian signed a document of informed consent, and patient verbal assent was obtained when appropriate. Following imaging at study enrollment, FDG-PET exams were performed annually. Patients were monitored by MRI and MRSI as clinically indicated or as outlined in the patient's treatment protocol. Patients who maintained eligibility remained on study up to 5 years.

MRI and MRSI

MRI was acquired on a Signa HDx 1.5T scanner with standard quadrature head coil (GE Healthcare, Milwaukee, WI). The majority of patients received intravenous propofol for sedation during MRI. Standard MR sequences included pre- and post-contrast T1-weighted images (TR/TE = 450/13 ms, FOV = 220 × 220 mm, matrix 256 × 192, slice thickness 3 mm), T2-weighted (TR/TE = 3,400/95 ms, FOV = 220 × 220 mm, matrix = 256 × 192, slice thickness = 3 mm) and fluid attenuated inversion recovery (FLAIR; TR/TE/TI = 10,000/140/2,200 ms, FOV = 220 × 220 mm, matrix = 256 × 192, slice thickness = 3 mm). Structural images were saved to our institution's picture archiving and communication system (PACS) for review by a neuroradiologist. Multi-slice MRSI was acquired prior to contrast administration using chemical shift selective water suppression, octagonal outer volume saturation, and a slice-selective spin echo sequence (TR/TE = 2,300/280 ms, FOV = 240 × 240 mm, matrix = 32 × 32, 4 slices, slice thickness = 15 mm, slice spacing = 3 mm, voxel size = 0.84 cm^3) as previously described [21], with slices placed for maximum coverage of the tumor.

Raw MRSI data were transferred to a workstation for processing and analysis using a customized software package developed in IDL (ITT Visual Information Solutions, Boulder, CO) [22], which provided automated peak selection and generation of signal intensity maps for the major metabolites including *N*-acetylaspartate (NAA), Choline (Cho) and Creatine. For each voxel within the signal intensity map, relative metabolite concentrations were reported as the integral of the area under each metabolite peak. Pre-contrast FLAIR images were

co-registered to MRSI as previously described [10, 23] and used as the anatomical reference. Regions of interest (ROIs) were manually drawn simultaneously on FLAIR and metabolite maps to include as much of the tumor as possible while avoiding areas of CSF, bone, and subcutaneous fat. For partially resected lesions, the remaining tumor and any portion of the surgical cavity perimeter with abnormal FLAIR signal were selected. ROI voxel locations were recorded using coordinates based on the 32 × 32 matrix from MRSI. Metabolite data were recorded and expressed as Cho:NAA ratios for ROI voxels which passed quality control measures including baseline appearance, metabolite peak separation, peak width, and lipid signal suppression as previously described [22].

FDG-PET

FDG-PET studies were performed using a GE Advance scanner (GE Healthcare). Patients fasted for ≥4 h for non-sedated scans and ≥8 h for sedated scans prior to FDG administration. The injected dose of 0.115 mCi/kg (maximum dose = 8.05 mCi) for all ages and body sizes, maintained a radiation exposure <0.5 rem, as required for pediatric research studies. FDG was given intravenously 45 min prior to scanning. Patients were positioned using a standard head support and thermoplastic facemask. Following transmission scan, the entire brain was imaged using a 3D emission scan, with 4.25 mm slice thickness. Attenuation correction was used for image reconstruction, with final 3D resolution of 6–7 mm full-width at half-maximum. Reconstructed PET images were sent to our institution's PACS for review. PET images were registered to T1-weighted post-contrast and pre-contrast FLAIR structural images from the corresponding MRI scan using a mutual-information, rigid body registration algorithm in MEDx 3.44 (Medical Numerics, Inc., Germantown, MD) [24].

Analysis of tumor activity

For MRSI, the maximum (Max) Cho:NAA from each ROI was used to classify tissue metabolic activity using the following schema (1) Max Cho:NAA <1 = inactive; 2) Max Cho:NAA ≥1 but ≤4.5 = active; 3) Max Cho:NAA >4.5 = highly active. Although there is no standardized classification of tumors based on proton spectroscopy, threshold values of Max Cho:NAA for this study were selected based on a previous study of MRSI biomarkers in pediatric patients with recurrent brain tumors [9]. For FDG-PET, T1-weighted post-contrast and pre-contrast FLAIR images were used for anatomical reference; PET and structural MRIs were reviewed side-by-side. Tumor activity was determined qualitatively by two experienced providers—a board certified neuroradiologist and the Chief of the PET department of our institution—using a visual comparison of the region with highest FDG-uptake within the tumor to normal grey and white matter (WM) from the contralateral side. For lesions with no normal contralateral tissue, such as brainstem gliomas, normal-appearing grey matter and WM from the frontal lobe at the level of the centrum semiovale was used for comparison. FDG-uptake within each lesion was classified using a 5-point grading system: grade 1 = less than contralateral WM; grade 2 = equal to contralateral WM; grade 3 = less than contralateral gray matter (GM) but greater than contralateral WM; grade 4 = equal to contralateral GM; grade 5 = greater than contralateral GM. These grades were consolidated into 3 categories of metabolic activity used for MRSI—(1) grade 1 or 2 = inactive; (2) grade 3 = active; (3) grade 4 or 5 = highly active. Both readers were blinded to patient diagnoses, outcomes and results of MRSI analysis. Readers evaluated scans independently then reviewed results together. If readers disagreed on FDG-PET tumor classification, the scan was classified as indeterminate and excluded from further analysis.

Voxel-wise analysis

We performed a voxel-wise analysis to identify the area of maximum tumor metabolic activity on FDG-PET and MRSI. The pre-contrast FLAIR registered to the MRSI data was the common anatomical reference for the two techniques. The location of Max Cho:NAA from MRSI was recorded using the MRSI ROI voxel coordinates. The FDG-PET was registered to the FLAIR using MEDx 3.44 (Medical Numerics, Inc.) [24]. Following registration, a grid of ROI voxels selected in the MRSI analysis was outlined on the FLAIR and PET images using the MRSI ROI voxel coordinates and a customized script in MEDx 3.44 (Fig. 1). FLAIR and FDG-PET images were evaluated side-by-side by a neuroradiologist blinded to the location of the voxel with Max Cho:NAA, and the brightest abnormal voxel within the ROI grid on the FDG-PET images was selected. The amount of tumor activity was not classified using the grading scales. To evaluate regional agreement of MRSI and FDG-PET, the location of the tumor voxel with the maximum metabolic activity on FDG-PET was compared to the location of the voxel with Max Cho:NAA on MRSI. Studies were considered in agreement if the voxel selected by FDG-PET was exactly the same or adjacent to the voxel selected by MRSI. Exact agreement was also assigned to studies in which lesions had no abnormal voxels or intensity of all voxels appeared equal of FDG-PET. Figure 1 illustrates regional agreement for 3 patients.

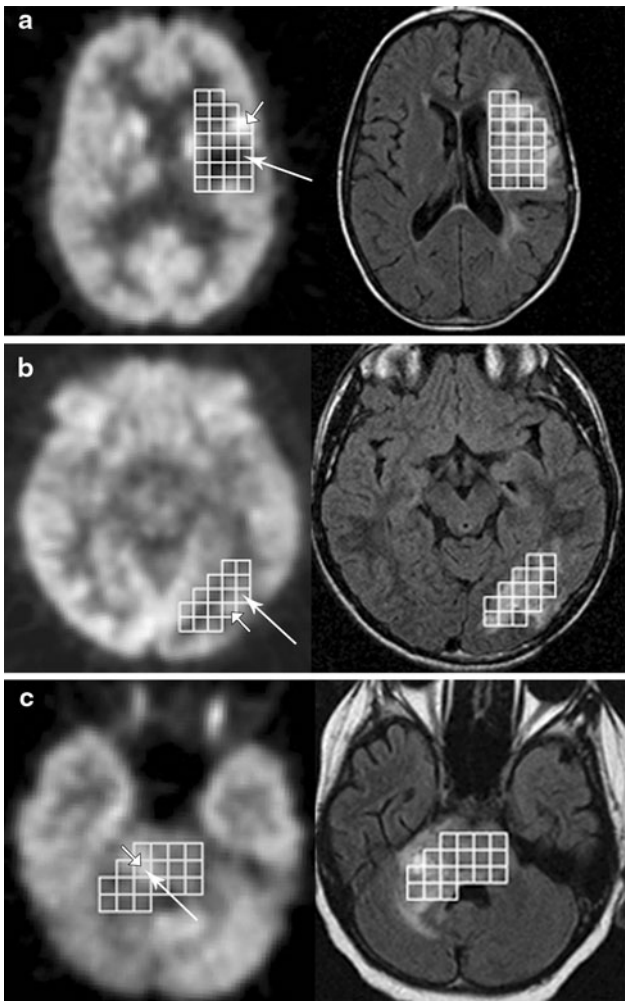

Fig. 1 Voxel-wise comparison of FDG-PEG and MRSI. FDG-PET (*left*) and FLAIR (*right*) images with the MRSI ROI voxels for 3 patients on study. Brightest voxel on PET indicated by *short arrow*. Voxel with Maximum Cho:NAA indicated by *long arrow*. **a** No agreement between MRSI and PET voxel selection. **b** and **c** Agreement between MRSI and FDG-PET. **b** Selected voxels are adjacent to one another and **c** the same voxel was chosen by both FDG-PET and MRSI

Statistical analysis

We evaluated agreement in the classification of tumor metabolism (inactive, active, and highly active) by FDG-PET and MRSI using overall percent agreement and the Kappa statistic (κ). Voxel-wise comparison between the two techniques was evaluated using overall percent agreement. The effect of tumor type and tumor size (determined by the number of ROI voxels) on the amount of agreement was also assessed using Mehta's modification to Fisher's exact Test and an exact Wilcoxon rank sum test, respectively. The brainstem contains both grey and WM structures, which are small (submillimeter) and have a similar appearance on MRI and PET. Thus ROI voxels from the brainstem likely contained contributions from both. To evaluate the effect of this partial volume contamination on agreement, we dichotomized the data by location (i.e., brainstem or outside the brainstem). The effect of tumor location on agreement was determined using a Fisher's exact test. p-Values were two-tailed and presented without adjustment for multiple comparisons. As each analysis was independent of all others in this exploratory analysis, all p values <0.05 were interpreted as being associated with statistically significant effects.

Results

Patients

At the time of analysis, 37 patients (15 male, 22 female) had enrolled on this study. Patient characteristics are listed in Table 1. The majority of patients were diagnosed with glioma. Twenty tumors (54 %) were located within the brainstem. FDG-PET and MRSI scans were performed within two weeks of one another (median = 1 day, range = 1–9 days). There was no change in any patient's clinical status between the FDG-PET and MRI scans. Only the initial scan for each patient was included in the comparison analysis, for a total of 37 paired studies.

Image analysis of MRSI and FDG-PET

For MRSI, metabolic data were obtained in all but one study, which was excluded due to significant baseline noise resulting in failed detection of metabolites. ROI sizes ranged from 4 to 46 voxels (median = 13). Metabolic data were obtained in the majority of ROI voxels (median = 81 %, range = 19–100 %). Max Cho:NAA values ranged from 0.7 to 6.7 (median = 1.8). For FDG-PET, one study was excluded from analysis after inadequate registration of the FDG-PET to the structural MRI. Readers evaluated the FDG-PET on the remaining 35 studies and reached a consensus on tumor metabolic activity for all but two studies, which were classified as indeterminate and removed from further analysis.

Agreement in tumor metabolic activity

Thirty-three paired FDG-PET and MRSI studies were available for agreement analysis (Table 2). The majority of tumors were active on MRSI ($n = 23$, 62 %), with only two meeting criteria for being highly active and eight classified as inactive. For FDG-PET, tumor classification was more widespread, with nearly equal numbers of metabolically active ($n = 9$) and highly active ($n = 10$) tumors. Fourteen tumors were classified as inactive on

Table 1 Patient characteristics ($n = 37$)

Characteristic	
Age at study enrollment–median (range)	12.3 years (3.1–21.7 years)
Tumor diagnosis	
Diffuse intrinsic pontine glioma (DIPG)	16 (43 %)
High-grade glioma (non-DIPG)	10 (27 %)
Low-grade glioma	10 (27 %)
Dysplastic gangliocytoma	1 (3 %)
Tumor location	
Posterior fossa	24 (65 %)
Supratentorial region	13 (35 %)
Surgical intervention ($n = 17$, 46 %)	
Biopsy	5 (14 %)
Resection[a] (gross total or partial)	12 (32 %)
Radiation therapy	23 (62 %)
Imaging at or during initial treatment	11 (30 %)
Imaging at recurrence or progression	11 (30 %)

[a] Patients who underwent gross total resection had suspected disease recurrence or residual disease at time of study enrollment

FDG-PET. Of these, eight (57 %) showed activity on MRSI, including one tumor that was highly active (Fig. 2). Overall agreement between FDG-PET and MRSI studies was 42 % (95 % CI, CI = 25–61 %). The Kappa statistic (κ) also showed weak agreement between the two techniques ($\kappa = 0.16$, $p = 0.12$ for test of whether $\kappa = 0$). Tumor location had no effect on agreement ($p > 0.05$).

Voxel-wise comparison

Thirty-five studies were included in the voxel-wise comparison of FDG-PET and MRSI—33 studies used in the tumor classification analysis with the addition of the two studies which were classified as indeterminate. One study was removed after inadequate registration between FDG-PET and FLAIR, for a total of 34 evaluable FDG-PET and MRSI studies. Overall agreement in selection of the voxel with maximum metabolic activity between the two techniques was 62 % (95 % CI = 43.6–77.8 %). The exact same voxel was selected by both FDG-PET and MRSI in 10 studies (29.4, 95 % CI = 15.1–47.5 %) (Fig. 1). Tumor location and tumor type had no effect on agreement ($p > 0.05$). However, smaller ROI size was significantly associated with agreement ($p = 0.011$).

Discussion

MRSI and FDG-PET are molecular imaging techniques used to evaluate the metabolism of brain tumors. This study evaluated the agreement of these techniques in (1) classification of the degree of tumor metabolism and (2)

Table 2 Classification of tumor metabolism

MRSI classification	FDG-PET classification		
	Inactive ($n = 14$)	Active ($n = 9$)	Highly active ($n = 10$)
Inactive ($n = 8$)	6	2	0
Active ($n = 23$)	7	7	9
Highly active ($n = 2$)	1	0	1

Underline indicates agreement between the two techniques (total = 14 cases)

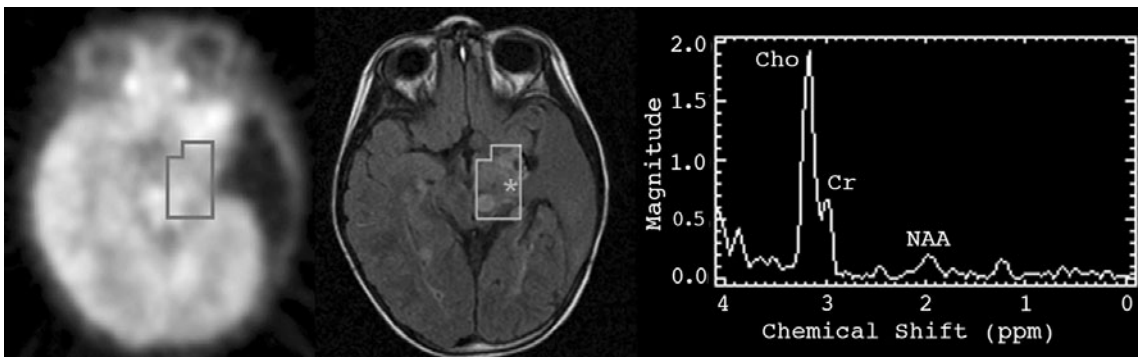

Fig. 2 Comparison of metabolic activity determined by FDG-PET and MRSI. Results obtained by MRSI (*right*) were classified as highly active (Max Cho:NAA = 6.7). Corresponding area on FDG-PET (*left*) was classified as inactive. Location of voxel with Max Cho:NAA is indicated by the *asterisk* on the pre-contrast FLAIR image (*center*)

identification of the most metabolically active region of the tumor. Metabolic activity on both MRSI and FDG-PET was heterogeneous across all tumor types, and in both analyses, agreement between FDG-PET and MRSI was weak. Although the majority of tumors had metabolic activity on MRSI and FDG-PET, the techniques differed in determining the degree of activity as determined by our classification method. Many tumors classified as active on MRSI were highly active on FDG-PET. The most striking finding in our study was the difference in the number of inactive lesions between each technique. MRSI showed activity in a majority of tumors that appeared inactive on FDG-PET studies.

The voxel-wise comparison of MRSI and FDG-PET yielded similar results. Overall, the percentage of studies with exact agreement was low (<30 %). However, the maximum voxels on FDG-PET and MRSI were either identical or adjacent to one another for the majority (62 %) of studies, indicating overlap in FDG-PET and MRSI for detecting tumor activity. Similarly, a recent analysis of functional and molecular MRI techniques, including MRSI, and FDG-PET in adults with high-grade gliomas found substantial overlap in selection of the most active tumor area [25]. This is not entirely unexpected given the poor spatial resolution of the two techniques. In our study, agreement in the area with the greatest metabolic activity was not associated with tumor location or a particular tumor type, but was associated with ROI size.

FDG-PET is the current standard of care for evaluating tumor metabolism in adults with brain tumors and is frequently used in pediatric oncology. Multi-slice CT with PET (PET/CT) is the most common method for acquiring FDG-PET, providing fusion of functional and structural images. In our study, FDG-PET images were co-registered and evaluated with structural MRIs. The benefits of this approach include high resolution of anatomic structure on multiple image types and reduced radiation exposure compared to standard PET/CT techniques. FDG-uptake for determining tumor malignancy can be challenging, with some overlap in the appearance of high-grade and low-grade lesions [19, 26] and decreased detection of tumor recurrence compared to other functional and molecular imaging techniques, including spectroscopy [27]. In our study, several lesions that appeared inactive on FDG-PET had increased metabolic activity on MRSI. Although MRSI has the advantages of using standard MRI equipment and not involving radiation exposure, application of MRSI in the clinical setting has been inhibited by a lack of standardization in acquisition and analysis methods [28–30]. Further analysis of FDG-PET and MRSI is warranted to determine which technique is more useful in assessing metabolic activity in children with brain tumors.

Study results should be interpreted with consideration to some limitations. Our objective was to determine agreement of metabolic classification between the two techniques at a single time point. While determining the association of FDG-PET and MRSI results with histology or tumor grade would strengthen the findings of this study, such an analysis was not performed due to the ethical limitations of obtaining tissue in these patients. Regions of edema, blood products and necrosis may be included in tumor analysis as these areas could not be distinguished from tumor on structural MRIs. Inclusion of normal-appearing tissue and CSF was avoided where possible in selection of tumor ROIs. However, despite the relatively high resolution of the MRSI technique (voxel resolution <1 cm^3), parital volume effects cannot be completely eliminated and CSF or surrounding normal tissues may have been contributed to MRSI tumor results. Patients enrolled on this study were heterogeneous in their diagnosis and treatment course, precluding correlation of imaging techniques with patient outcome or response. Selection of the Max Cho:NAA from MRSI was based on the metabolic data from voxels meeting quality control criteria, which in some cases was <100 % of the total ROI voxels. Therefore, Max Cho:NAA selected may not be representative of the most metabolically active voxel within the tumor due to very low NAA or poor quality spectra in regions susceptible to field inhomogeneity. Selection of Max Cho:NAA thresholds for metabolic classification were based on a previous study of recurrent brain tumors in children [9]. In our study, few highly active tumors were identified by MRSI. Evaluation of MRSI in pediatric CNS tumors with histological validation of tumor grade when possible is warranted to improve threshold selection and tumor stratification.

Conclusion

While both MRSI and FDG-PET are useful techniques for evaluating tumor metabolism, we found low agreement between the metabolic activity on FDG-PET and the Max Cho:NAA detected by MRSI in pediatric brain tumors.

Acknowledgments This work was presented in part at the 2011 ASCO annual meeting in Chicago, IL. The views expressed in this article are those of the authors and do not reflect the official policy of the National Institutes of Health, Department of Army, Department of Defense, or U.S. Government. Research was supported in part by the Intramural Research Program of the National Institutes of Health, National Cancer Institute, Center for Cancer Research.

References

1. Pollack IF, Jakacki RI (2011) Childhood brain tumors: epidemiology, current management and future directions. Nat Rev Neurol 7:495–506

2. Central Brain Tumor Registry of the United States (CBTRUS) (2010) CBTRUS statistical report: primary and central nervous system tumors diagnosed in the United States in 2004–2006. CBTRUS, Hindsdale, pp 10–25
3. Verma R, Zacharaki EI, Ou Y, Cai H, Chawla S, Lee SK, Melhem ER, Wolf R, Davatzikos C (2008) Multiparametric tissue characterization of brain neoplasms and their recurrence using pattern classification of MR images. Acad Radiol 15:966–977
4. Yang I, Huh NG, Smith ZA, Han SJ, Parsa AT (2010) Distinguishing glioma recurrence from treatment effect after radiochemotherapy and immunotherapy. Neurosurg Clin N Am 21: 181–186
5. Peet AC, Lateef S, MacPherson L, Natarajan K, Sgouros S, Grundy RG (2007) Short echo time 1 H magnetic resonance spectroscopy of childhood brain tumours. Childs Nerv Syst 23: 163–169
6. Astrakas LG, Zurakowski D, Tzika AA, Zarifi MK, Anthony DC, De Girolami U, Tarbell NJ, Black PM (2004) Noninvasive magnetic resonance spectroscopic imaging biomarkers to predict the clinical grade of pediatric brain tumors. Clin Cancer Res 10: 8220–8228
7. Tzika AA, Astrakas LG, Zarifi MK, Zurakowski D, Poussaint TY, Goumnerova L, Tarbell NJ, Black PM (2004) Spectroscopic and perfusion magnetic resonance imaging predictors of progression in pediatric brain tumors. Cancer 100:1246–1256
8. Marcus KJ, Astrakas LG, Zurakowski D, Zarifi MK, Mintzopoulos D, Poussaint TY, Anthony DC, De Girolami U, Black PM, Tarbell NJ, Tzika AA (2007) Predicting survival of children with CNS tumors using proton magnetic resonance spectroscopic imaging biomarkers. Int J Oncol 30:651–657
9. Warren KE, Frank JA, Black JL, Hill RS, Duyn JH, Aikin AA, Lewis BK, Adamson PC, Balis FM (2000) Proton magnetic resonance spectroscopic imaging in children with recurrent primary brain tumors. J Clin Oncol 18:1020–1026
10. Steffen-Smith EA, Shih JH, Hipp SJ, Bent R, Warren KE (2011) Proton magnetic resonance spectroscopy predicts survival in children with diffuse intrinsic pontine glioma. J Neurooncol 105: 365–373
11. Padma MV, Said S, Jacobs M, Hwang DR, Dunigan K, Satter M, Christian B, Ruppert J, Bernstein T, Kraus G, Mantil JC (2003) Prediction of pathology and survival by FDG PET in gliomas. J Neurooncol 64:227–237
12. Di Chiro G (1987) Positron emission tomography using [18F] fluorodeoxyglucose in brain tumors. A powerful diagnostic and prognostic tool. Invest Radiol 22:360–371
13. Patronas NJ, Di Chiro G, Kufta C, Bairamian D, Kornblith PL, Simon R, Larson SM (1985) Prediction of survival in glioma patients by means of positron emission tomography. J Neurosurg 62:816–822
14. Alavi JB, Alavi A, Chawluk J, Kushner M, Powe J, Hickey W, Reivich M (1988) Positron emission tomography in patients with glioma. A predictor of prognosis. Cancer 62:1074–1078
15. Ogawa T, Uemura K, Shishido F, Yamaguchi T, Murakami M, Inugami A, Kanno I, Sasaki H, Kato T, Hirata K et al (1988) Changes of cerebral blood flow, and oxygen and glucose metabolism following radiochemotherapy of gliomas: a PET study. J Comput Assist Tomogr 12:290–297
16. Imani F, Boada FE, Lieberman FS, Davis DK, Deeb EL, Mountz JM (2010) Comparison of proton magnetic resonance spectroscopy with fluorine-18 2-fluoro-deoxyglucose positron emission tomography for assessment of brain tumor progression. J Neuroimaging [Epub ahead of print 14 Dec 2010]
17. Zukotynski KA, Fahey FH, Kocak M, Alavi A, Wong TZ, Treves ST, Shulkin BL, Haas-Kogan DA, Geyer JR, Vajapeyam S, Boyett JM, Kun LE, Poussaint TY (2011) Evaluation of 18F-FDG PET and MRI associations in pediatric diffuse intrinsic brain stem glioma: a report from the pediatric brain tumor consortium. J Nucl Med 52:188–195
18. Pirotte B, Acerbi F, Lubansu A, Goldman S, Brotchi J, Levivier M (2007) PET imaging in the surgical management of pediatric brain tumors. Childs Nerv Syst 23:739–751
19. Utriainen M, Metsahonkala L, Salmi TT, Utriainen T, Kalimo H, Pihko H, Makipernaa A, Harila-Saari A, Jyrkkio S, Laine J, Nagren K, Minn H (2002) Metabolic characterization of childhood brain tumors: comparison of 18F-fluorodeoxyglucose and 11C-methionine positron emission tomography. Cancer 95:1376–1386
20. Borgwardt L, Hojgaard L, Carstensen H, Laursen H, Nowak M, Thomsen C, Schmiegelow K (2005) Increased fluorine-18 2-fluoro-2-deoxy-D-glucose (FDG) uptake in childhood CNS tumors is correlated with malignancy grade: a study with FDG positron emission tomography/magnetic resonance imaging coregistration and image fusion. J Clin Oncol 23:3030–3037
21. Duyn JH, Gillen J, Sobering G, van Zijl PC, Moonen CT (1993) Multisection proton MR spectroscopic imaging of the brain. Radiology 188:277–282
22. Tedeschi G, Bertolino A, Campbell G, Barnett AS, Duyn JH, Jacob PK, Moonen CT, Alger JR, Di Chiro G (1996) Reproducibility of proton MR spectroscopic imaging findings. AJNR Am J Neuroradiol 17:1871–1879
23. Hipp SJ, Steffen-Smith E, Hammoud D, Shih JH, Bent R, Warren KE (2011) Predicting outcome of children with diffuse intrinsic pontine gliomas using multiparametric imaging. Neuro-oncol 13: 904–909
24. Jenkinson M, Smith S (2001) A global optimisation method for robust affine registration of brain images. Med Image Anal 5: 143–156
25. Weber MA, Henze M, Tuttenberg J, Stieltjes B, Meissner M, Zimmer F, Burkholder I, Kroll A, Combs SE, Vogt-Schaden M, Giesel FL, Zoubaa S, Haberkorn U, Kauczor HU, Essig M (2010) Biopsy targeting gliomas: do functional imaging techniques identify similar target areas? Invest Radiol 45:755–768
26. Fulham MJ, Melisi JW, Nishimiya J, Dwyer AJ, Di Chiro G (1993) Neuroimaging of juvenile pilocytic astrocytomas: an enigma. Radiology 189:221–225
27. Prat R, Galeano I, Lucas A, Martinez JC, Martin M, Amador R, Reynes G (2010) Relative value of magnetic resonance spectroscopy, magnetic resonance perfusion, and 2-(18F) fluoro-2-deoxy-D-glucose positron emission tomography for detection of recurrence or grade increase in gliomas. J Clin Neurosci 17: 50–53
28. Parmar H, Lim TC, Yin H, Chua V, Khin LW, Raidy T, Hui F (2005) Multi-voxel MR spectroscopic imaging of the brain: utility in clinical setting-initial results. Eur J Radiol 55:401–408
29. Mandal PK (2011) In vivo proton magnetic resonance spectroscopic signal processing for the absolute quantitation of brain metabolites. Eur J Radiol [Epub ahead of print 22 Apr 2011]
30. Horska A, Barker PB (2010) Imaging of brain tumors: MR spectroscopy and metabolic imaging. Neuroimaging Clin N Am 20:293–310